Published in
Applied Physics B : Lasers and Optics 100, issue 2, 321-329, 2010
which should be used for any reference to this work

Spectral and modulation properties of a largely tunable MEMS-VCSEL in view of gas phase spectroscopy applications

S. Schilt · K. Zogal · B. Kögel · P. Meissner · M. Maute · R. Protasio · M.-C. Amann

Abstract An extensive characterization of the spectral properties of a largely tunable laser in the 1.56-μm spectral range is reported. This device combines a vertical-cavity surface-emitting laser (VCSEL) with a micro-machined (MEMS) Bragg mirror in a very compact arrangement. The large tunability obtained by an electro-thermal actuation of the MEMS mirror makes this device very attractive for high-resolution spectroscopy. Relevant laser parameters for the implementation of wavelength modulation spectroscopy techniques in gas sensing, such as tuning and modulation properties, are presented. A preliminary gas spectroscopy experiment performed with this laser is also shown.

S. Schilt (✉) · R. Protasio
IR Microsystems SA, PSE-C, 1015 Lausanne, Switzerland
e-mail: stephane.schilt@unine.ch
Fax: +41-21-7182511

Present address:
S. Schilt
Laboratory for Time and Frequency, Institute of Physics,
University of Neuchâtel, 2009 Neuchâtel, Switzerland

K. Zogal · B. Kögel · P. Meissner
Fachgebiet Optische Nachrichtentechnik, Technische Universität
Darmstadt, Merckstrasse 25, 64283 Darmstadt, Germany

Present address:
B. Kögel
Department of Microtechnology and Nanoscience, Chalmers
University of Technology, 412 96 Göteborg, Sweden

M. Maute · M.-C. Amann
Walter Schottky Institut, Technische Universität München,
Am Coulombwall, 85748 Garching, Germany

1 Introduction

Widely- and fast-tunable lasers find applications in many different areas, such as optical telecommunications, atomic or molecular spectroscopy [1–3], or optical sensing [4]. In industrial gas sensing applications, for instance, a broad tuning range enables to address several molecules with a single laser source, facilitating selective multigas monitoring of heterogeneous gas samples alongside with the remote extraction of process parameters, such as temperature and pressure, in a simple and cost-effective configuration. Current technologies to achieve a large tunability include the use of an external cavity or the combination of a large number of diode lasers, each of them having a limited tuning range.

External cavity diode lasers (ECDL) are routinely used in spectroscopy [1, 5], in optical telecommunications [6, 7], or in instrumentation. This mature technology is commercially available for a long time and has been extended to mid-infrared quantum cascade lasers for a few years [8, 9]. In these systems, the broad gain curve of a Fabry–Perot diode laser is combined with a mechanically adjustable Bragg-grating cavity to provide a large tunability, which can amount up to 15% of the central wavelength [9]. In addition to the large tunability, the external grating cavity also provides single-mode emission with a narrow instantaneous linewidth (typ. $<$ a few 100 kHz). Additionally, a large optical power (up to 100 mW continuous wave) is achievable in an ECDL [9]. However, these lasers need a very precise alignment of the external cavity to achieve mode-hop-free tuning, which makes external-cavity-based lasers expensive. The tuning is usually performed by the combined use of a stepper motor (for coarse wavelength adjustment) and a piezo-transducer (for fine adjustment). Other disadvantages of ECDLs are their large size compared to semiconductor

diode lasers and the relative sensitivity of the external cavity to vibrations and acoustic noise, which increases the flicker ($1/f$) noise of the laser both in terms of intensity noise and frequency noise. As a consequence, an additional stabilization loop (e.g., using an atomic or molecular absorption line) may be necessary in some applications requiring very-high stability [10]. Finally, tuning of an ECDL over a large range is usually quite slow, as it is a mechanical process accomplished with the stepper motor.

Another type of commercially available system in the optical telecommunication spectral range (S-, C-, and L-band), which is worth to mention, is made up of an array of several (typ. 8–16) slightly detuned DFB laser chips. The lasers are coupled into an optical fiber using a MEMS mirror [11] or a passive optical combiner [12]. Owing to the individual 3–4-nm tuning range of a single DFB laser and to the number of different lasers integrated in these devices, a total tuning range of up to ∼40 nm is achievable, with a typical output power of 10–50 mW. This tuning is achieved by activating a particular element of the array (coarse tuning) and by adjusting the laser temperature (medium tuning) and the injection current (fine tuning). Since all the chips are generally mounted on the same thermoelectric cooler, tuning over a large range is usually quite slow. Additionally, the number of DFB chips needed to reach the large tuning range makes these systems costly.

In this paper, we report on an alternative type of widely tunable laser obtained by combining two technologies in an integrated device, namely a vertical-cavity surface-emitting laser (VCSEL) and a micro-machined (MEMS) movable Bragg mirror membrane. This so-called MEMS-VCSEL technology combines the main advantages of VCSELs (inherent longitudinal single-mode behavior, compactness, low power consumption, etc.) with the large tunability provided by the thermal actuation of the membrane which acts as a movable external mirror. The potential advantages of the reported technology comprise a very compact size incorporable into a TO-package as commonly used for standard laser diodes, a tuning range of several tens of nanometers provided by an electro-thermal or electrostatic actuation of the membrane and a fast tuning over the entire range at millisecond timescales. A continuous static tuning range scaling up to 60 nm has been previously demonstrated for MEMS-VCSELs in the optical telecommunications C-band [2] with a 3-dB tuning bandwidth of 180 Hz [3, 13]. To achieve such a large tunability, the device is designed to operate in a so-called extended-cavity configuration, in which the top facet of the half-VCSEL is anti-reflection-coated to prevent a residual reflection at the semiconductor–air interface so as to deal with a single optical cavity between the bottom distributed Bragg reflector (DBR) and the MEMS mirror. The work reported here shows preliminary results obtained in the frame of the European project Subtune.[1] The main objectives of this development are: (1) to enlarge the spectral coverage of this type of MEMS-VCSEL to both shorter (down to 800 nm) and longer (up to 2.1 μm) wavelength using GaAs and InP materials, respectively; (2) to increase the tuning frequency (full spectral scan) to ∼100 kHz; (3) to ensure well-defined polarization stability using a sub-wavelength grating. These developments are performed in close connection with different applications of interest for these lasers, namely optical telecommunications, fiber Bragg grating sensor interrogation, and gas sensing, in order to fulfil their respective requirements. In this paper, we focus on the gas sensing application and we present some properties of a 1.56-μm MEMS-VCSEL that are relevant in view of the future application of this device in wavelength modulation spectroscopy (WMS). In particular, the tuning and modulation characteristics of the device are shown, as well as preliminary results of gas spectroscopy obtained with this laser.

2 Laser design and fabrication

The tunable VCSEL is a hybrid two-chip assembly of a micro-electro-mechanical system with concave AlGaAs/GaAs mirror membrane and an InP-based semiconductor cavity with a tunnel junction aperture [13, 14]. The MEMS technology is very promising in respect to the achievement of very good spectral properties. By the use of a half-symmetric resonator, the fundamental Gaussian mode of the laser can be supported. Essential for this approach is the coincidence of the phase of the optical beam with the curvature of the membrane (see Fig. 1). The included air-gap can be expanded by using the electro-thermal MEMS actuation and the cavity resonance can be tuned to a longer wavelength.

Figure 2a presents the schematic of the tunable MEMS-VCSEL showing the upper movable Bragg mirror with the actuating contacts, an air-gap, the semiconductor cavity, and the bottom mirror terminated with a gold p-contact, which additionally provides efficient heat exchange. The top DBR consists of molecular beam epitaxy grown GaAs/AlGaAs effective quarter wavelength layers with a difference in refractive index of 0.39. The concave bending of the membrane is caused by targeted mechanical compressive strain embedded into the DBR layers during the epitaxial deposition of the material. The inclusion of indium up to 5% at the upper part of the mirror causes a slight lattice mismatch of GaAs/AlGaAs layers which then results in a membrane deflection within the range of 6–12 μm (air-gap) and a radius of curvature within the range of 2–3 mm. The MEMS-VCSEL used in this work has an air-gap of 6.1 μm and a

[1] www.subtune.eu.

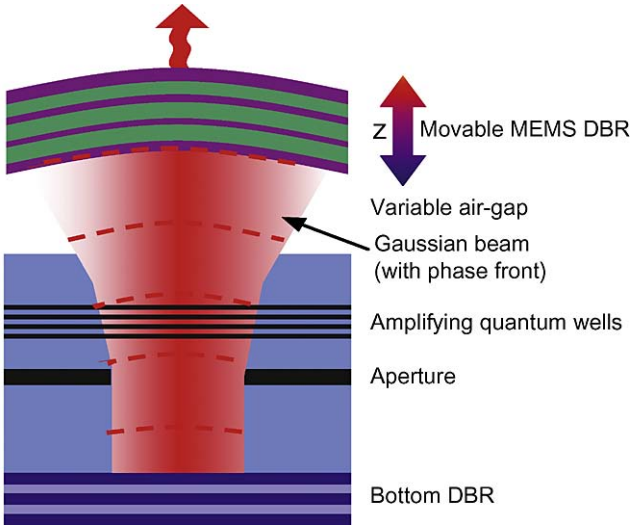

Fig. 1 The half-symmetric VCSEL resonator with concave bended top DBR (distributed Bragg reflector)

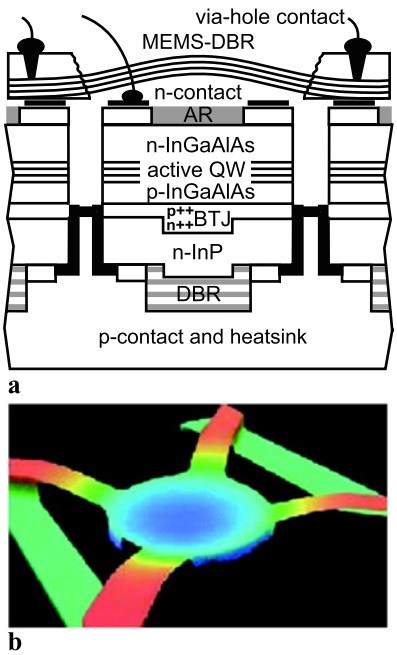

Fig. 2 (**a**) Cross-section view of the MEMS tunable VCSEL. (**b**) Confocal microscope 3D picture of the membrane

membrane diameter of 190 µm. Additionally, the semiconductor DBR layers are doped with silicon during the epitaxial process to enable an electrical conductivity and thus tuning of the membrane. The current flowing through via-holes contacts causes power dissipation in the membrane and thus temperature increase which is then responsible for the elongation of the four membrane support beams (89 µm length × 50 µm width) and mirror bending. Owing to the symmetric four-beam design, the deflection remains stable and there is no tilt of the membrane which would cause

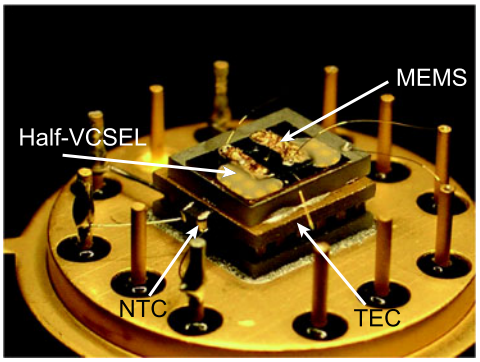

Fig. 3 Assembly of the MEMS-VCSEL into a T08-package with an active temperature control. TEC: thermoelectric cooler; NTC: negative temperature coefficient thermistor

losses in the resonator (see Fig. 2b). The membrane resistivity is 340 Ω. The active region consists of seven compressively strained InGaAlAs quantum wells embedded between an n-type and a thin p-type InGaAlAs confinement layer. A centrally limited buried tunnel junction aperture (Ø 10–20 µm) defines the active size of the laser. The dielectric bottom DBR consists of 3.5 pairs of evaporated calcium fluoride and zinc sulphide (CaF_2/ZnS) with a gold coating and an electroplated substrate. Such back mirror has limited size, slightly larger than the buried tunnel junction aperture.

In the reported experiments a tunable VCSEL in a semiconductor-coupled-cavity configuration is used, i.e., without anti-reflection coating on the top facet of the half-VCSEL. The optical thickness of the semiconductor cavity is $22\lambda/4$ and the buried tunnel junction diameter is 10 µm. The optical length of the resonator is $L_0 = 16.66$ µm ($22\lambda/4$ semiconductor cavity + $2.5\lambda/4$ back mirror + 1-µm penetration depth of the optical field into the MEMS-DBR + 6.1-µm air-gap), which corresponds to the calculated free spectral range (FSR) of the laser of 73 nm. However, the measured FSR in our tunable VCSELs without an anti-reflection coating is 39.8 nm. The deviation is caused by the coupled cavities (the uncoated interface forms a third mirror inside the cavity), which makes the previous simple calculation imprecise. A valid calculation of the FSR in a coupled-cavity VCSEL would require a 1D simulation. However, an "effective" cavity length of $L_{\text{eff}} = 30$ µm can be derived from the measured value of the FSR in our VCSEL.

The laser emits up to 1 mW of optical power in continuous-wave operation at room temperature (20°C). Half VCSEL and MEMS are fixed after active alignment using UV-curable adhesive. The laser is mounted in a TO-8 package with an integrated thermoelectric cooler. In these preliminary experiments, the TO package is kept open, i.e., it is not sealed with a protective window. A fully assembled and packaged MEMS-tunable VCSEL is shown in Fig. 3.

3 Laser characterization

Spectral, tuning, and modulation characteristics are important properties of a laser in view of its application to gas phase high-resolution spectroscopy, such as trace gas sensing. Spectral purity and tunability are both needed for high selectivity sensing: spectral purity (i.e., single-mode emission) enables a gas absorption line to be probed with a narrowband, ideally monochromatic radiation; tunability is required either to precisely adjust the laser wavelength at a fixed required value, which usually coincides with the center of the analyzed absorption line in line-locked mode of operation, or to scan the laser through the absorption line in a scan mode. In the case of a largely tunable laser for multigas sensing, the tunability should enable to simultaneously scan several lines of different species or to quickly switch between lines of different species. The modulation capabilities of the laser are important to implement modulation-based sensitive detection techniques, such as wavelength modulation spectroscopy (WMS, [15, 16]) or frequency modulation spectroscopy (FMS, [17, 18]). A relevant parameter in these techniques is the frequency (or wavelength) modulation that is induced by a direct modulation of the laser. In the MEMS-VCSEL, high-frequency modulation may be applied to the laser injection current just as in the case of standard laser diodes. Additionally, modulation of the membrane current is also applicable but with a much lower bandwidth.

The tuning properties of the MEMS-VCSEL have been measured using a wavemeter (Burleigh WA-1000) with 1-pm resolution, while spectral and modulation properties have been measured using a high-resolution (0.01 nm) optical spectrum analyzer (OSA, Advantest Q8384). For all these measurements, the output power of the VCSEL is coupled into a single-mode optical fiber pigtail. The laser temperature remains constant at $T = 20°C$ and the laser and membrane current varies throughout the experiments.

3.1 Spectral and tuning properties

The spectrum of the MEMS-VCSEL obtained at different membrane currents and at constant laser injection current $I_{\text{laser}} = 18$ mA is shown in Fig. 4a. One can notice that the laser emission initiates at $I_{\text{MEMS}} = \sim 5$ mA. This is due to slightly mismatched membrane air-gap. The laser emission is present up to $I_{\text{MEMS}} = \sim 14.5$ mA. The corresponding spectral coverage is ~1552–1572 nm with >50 dB side-mode suppression ratio (SMSR) of higher order transverse and longitudinal modes. The total continuous static tuning range is thus ~20 nm. This is yet a factor 2–3 smaller than previous performances achieved for similar MEMS-VCSELs [2, 3]. For the considered laser semiconductor-coupled-cavity configuration, the free spectral range is typical 15–20 nm smaller compared to an extended-cavity design with the same optical length L_0. This results from the simple resonator theory: $FSR = \lambda^2/2L_{\text{eff}}$, where $L_{\text{eff}} = \sum n_i L_i$ is the effective optical length of the resonator that takes into account the refractive index n_i in each section L_i of the cavity, weighted by the corresponding field intensity [19]. In the extended-cavity design, the field intensity is higher in the air-gap than in the semiconductor cavity owing to the presence of the anti-reflection coating while these fields are of similar amplitude in the coupled-cavity configuration [19]. Therefore, the air-gap section that exhibits a small refraction index has a stronger contribution to the effective optical length L_{eff} in an extended-cavity configuration than in a coupled-cavity. In a comparative study of the two types of configurations for an almost identical physical dimension [19], a FSR of 58 nm was obtained for the extended-cavity configuration (corresponding to $L_{\text{eff}} = 20.7$ µm) compared to 42 nm in the coupled-cavity ($L_{\text{eff}} = 28.5$ µm). Additionally the gain spectral distribution together with the cavity length define the upper limitation of the tuning range.

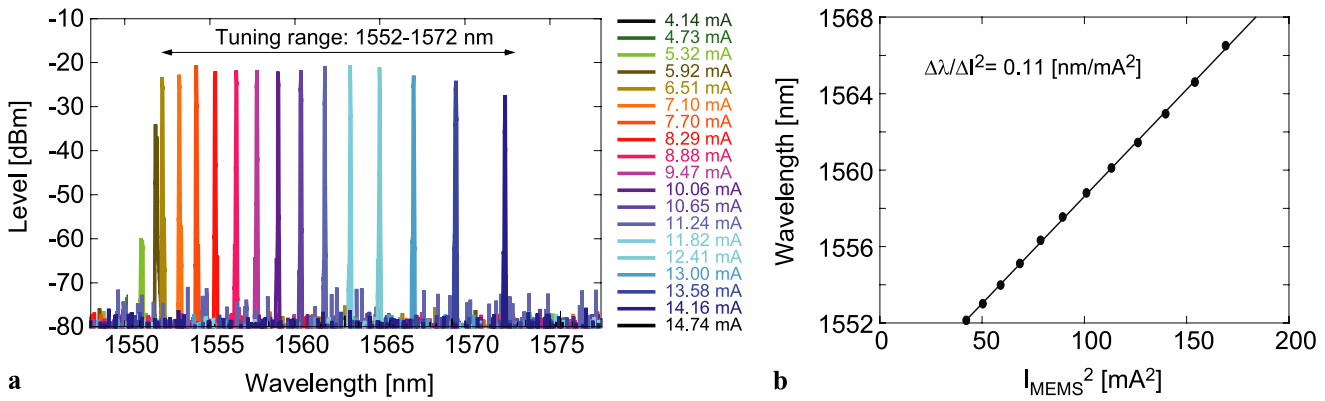

Fig. 4 (**a**) Superimposed spectra of the MEMS-VCSEL obtained at different membrane bias currents ($I_{\text{laser}} = 18$ mA). A total spectral range of 20 nm (1552–1572 nm) is covered by the laser with SMSR > 50 dB. (**b**) Dependency of the laser wavelength as a function of the squared membrane bias current. *Points* represent experimental data and *the line* is the result of a linear fit

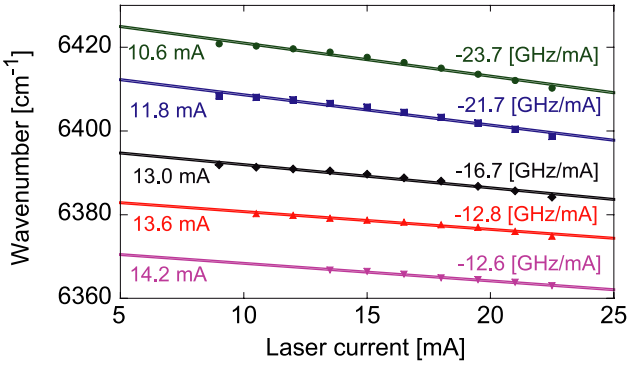

Fig. 5 Static tuning as a function of the laser injection current at different membrane bias currents. Measurement performed with an optical spectrum analyzer with the laser temperature stabilized at $T = 20°C$

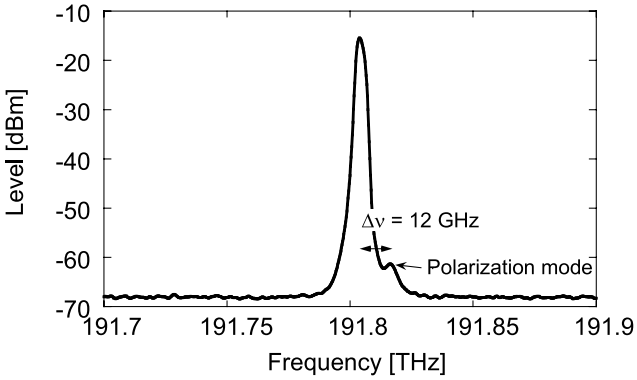

Fig. 6 The high-resolution view of the laser spectrum showing a small (PMSR > 40 dB) polarization mode shifted ∼12 GHz from the main peak. Measurement obtained at $T_{\text{laser}} = 20°C$, $I_{\text{laser}} = 21$ mA, $I_{\text{MEMS}} = 11.8$ mA

The laser wavelength scales quite linearly with the square of the membrane current (with an average slope of 0.11 nm/mA^2), as expected for a thermal actuation (see Fig. 4b). But higher order nonlinearities are known to occur in MEMS-VCSELs operated in semiconductor-coupled-cavity configurations and a closer look at the tuning curve shows a weak inverted s-shaped dependence that is characteristic of these devices [20]. Coarse adjustment of the laser wavelength is thus performed by the electro-thermal actuation of the MEMS membrane. Finer adjustments may be achieved through the laser injection current as shown in Fig. 5. Tuning with injection current is also essentially a thermal effect characterized by a quadratic response curve. However, the nonlinearity is weak in that case so that the observed laser emission frequency scales almost linearly with the laser injection current, at a rate that depends on the MEMS bias current: the laser tuning coefficient $\Delta\nu/\Delta I_{\text{laser}}$ tends to decrease with increasing MEMS bias current. This behavior results from the fact that static or low-frequency tuning with laser injection current is mainly a thermally-induced effect: the optical length of the semiconductor cavity expands with increasing injection current due to heating (resulting from the combination of a dilatation of the physical length of the cavity and an increase of the medium refractive index, which is the dominant process), which shifts the wavelength to longer values. The important parameter that governs the laser current tuning coefficient is the relative expansion of the entire cavity formed between the bottom DBR and the membrane mirror. This cavity is composed of two subsections, the semiconductor half-VCSEL and the air-gap. The absolute expansion of the first subsection (semiconductor cavity) may be considered as constant for a given injection current variation whatever is the MEMS current. But the second subpart (air-gap) extends with the MEMS current due to the membrane deformation. As a result, the relative expansion of the entire laser cavity due to a variation of the injection current drops with the MEMS current, and so does the laser injection current tuning coefficient. Values ranging from −24 to −12 GHz/mA have been obtained in static mode, which is typically 4–5 times smaller than the tuning rate of standard VCSELs in the same spectral range [21, 22].

A closer view of the laser peak obtained at $I_{\text{laser}} = 21$ mA is shown in Fig. 6. A very small (∼45 dB attenuation) lateral peak is observed ∼12 GHz away from the main peak. This tiny mode corresponds to the orthogonal polarization mode, which, however, does not affect the general behavior of the laser since the polarization remains stable (no polarization mode switching or partition) and shows a stable polarization mode suppression ratio of PMSR > 40 dB. The resolution of the measured spectrum is insufficient to resolve the laser linewidth, but previous measurements obtained by the delayed self-heterodyne technique on a similar type of MEMS-VCSEL have shown a linewidth in the 30-MHz range [23].

3.2 Frequency modulation characteristics

The frequency modulation (FM) characteristics of the laser have been quantified for a modulation of either the laser injection current or the membrane current. In all cases, a modulation of a varying amplitude or frequency is applied to the device (through the injection current or membrane current). The amplitude $\Delta\nu$ of the induced FM is determined from the optical spectrum, measured with the high-resolution OSA. The determination of the FM amplitude is based on a similar principle commonly used to measure the laser FM response using a scanning Fabry–Perot interferometer [24]. In the case of a high FM index as encountered in our experiments (a low modulation frequency in conjunction with a large instantaneous frequency deviation $\Delta\nu$), the observed modulation spectrum shows a typical U-shape and the frequency interval between the two maxima of this spectrum is a direct measurement of the peak-to-peak instantaneous frequency deviation ($2\Delta\nu$) of the laser (see Fig. 7).

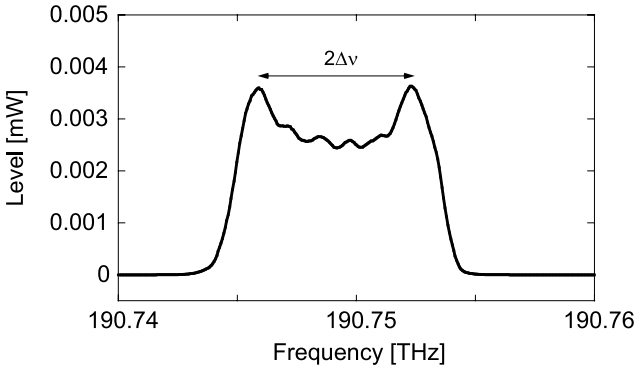

Fig. 7 Example of a laser FM spectrum measured with the optical spectrum analyzer ($I_{\text{laser}} = 21$ mA, $I_{\text{MEMS}} = 14.1$ mA, laser injection current modulation at $f = 25$ kHz, peak-to-peak amplitude 0.46 mA). The peak-to-peak variation of the laser instantaneous frequency ($2\Delta\nu = 6.6$ GHz) corresponds to the distance between the two maxima of the U-shape spectrum

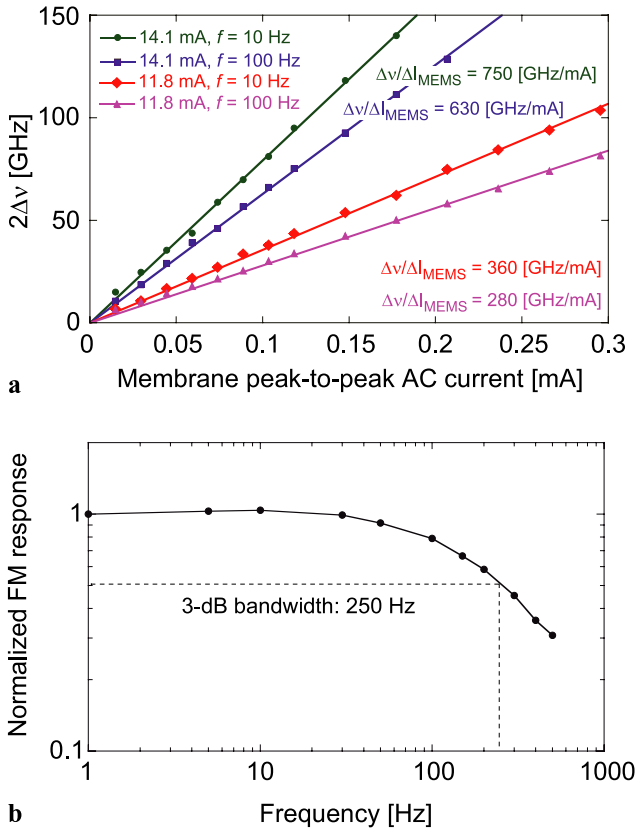

Fig. 8 (**a**) Amplitude of the laser FM as a function of the membrane AC current obtained at two different modulation frequencies (10 Hz and 100 Hz) and for two MEMS bias currents ($I_{\text{MEMS}} = 11.8$ mA and $I_{\text{MEMS}} = 14.1$ mA). (**b**) Frequency response of the MEMS modulation. The 3-dB bandwidth is 250 Hz

Modulation of the MEMS current was investigated at a constant laser injection current $I_{\text{laser}} = 18$ mA and at two different modulation frequencies, $f = 10$ Hz and $f = 100$ Hz. Figure 8a shows that the amplitude of the laser FM scales linearly with the amplitude of the AC current applied to the membrane. The tuning coefficient has some dependence on the membrane bias current: the tuning is approximately two times larger at $I_{\text{MEMS}} = 14.1$ mA than at $I_{\text{MEMS}} = 11.8$ mA. The effect of the bandwidth of the membrane modulation is also apparent in this plot, since the FM response is typically 20% lower at $f = 100$ Hz compared to $f = 10$ Hz. The frequency response of the membrane is shown in more details in Fig. 8b: a 3-dB bandwidth of 250 Hz is achieved. The electro-thermal actuation of the membrane thus enables to scan large spectral interval (up to the entire spectral coverage of the laser) in <10 ms timescale or to quickly switch between different distant wavelengths in the range of 10–20 nm for the present laser (or up to 50 nm for MEMS-VCSELs with a larger tuning range as reported in [2, 3]). These features are very attractive for multigas sensing.

Much faster modulation is achievable by modulating the laser injection current but with a strongly reduced spectral extend, which can nevertheless cover a few hundred gigahertz for a large variation of the laser current. This is usually by far sufficient to scan over one or a few neighboring absorption lines at atmospheric pressure, where lines have a typical width of a couple of GHz. For a (small) modulation of the laser injection current at ~25 kHz an almost linear FM response is obtained, as shown in Fig. 9. Here again, an influence of the membrane bias current is observed on the laser FM response. The tuning coefficient is more or less constant ($\Delta\nu/\Delta I = \sim 30$ GHz/mA in this case) up to $I_{\text{MEMS}} = \sim 12$ mA but it drops at higher MEMS bias current. The origin of this behavior is similar to the case of the static tuning with the laser injection current at different membrane bias currents discussed in Fig. 5. The highest value of the AC tuning coefficient observed in Fig. 9 compared to the static tuning previously shown in Fig. 5 is due to different laser injection currents (18 mA in Fig. 5 vs. 21 mA in Fig. 9). It is well known that the tuning coefficient of a VCSEL increases significantly with the laser DC current [21].

4 Preliminary gas spectroscopy results

Preliminary gas sensing experiments have been performed with our MEMS-VCSEL in order to evaluate the potential of such a light source for high-resolution spectroscopy. The experimental scheme used in this experiment is depicted in Fig. 10. Light emitted from the MEMS-VCSEL is coupled into a single-mode optical fiber, which facilitates the acquisition of additional spectral measurements using the OSA without modifying the setup. At the fiber exit, the light is collimated and transmitted through a single-pass 1-m long absorption cell sealed with Brewster-angled BK7 windows. The transmitted light is finally detected with a

photodiode. Pure carbon dioxide (CO_2) is used as a test gas for preliminary WMS measurements. WMS is implemented using a custom electronics board that was originally developed for cost-effective gas sensors based on standard VCSELs. This home-designed electronics performs laser current and temperature control, injection current modulation at ∼25 kHz, second-harmonic ($2f$) lock-in demodulation, and slow (step-by-step) scans of the laser DC current to measure the direct absorption signal or the $2f$ spectrum. The control of the membrane bias current is done externally using a laboratory current source.

Figure 11a shows an example of the observed $2f$ spectrum of a CO_2 absorption line. A characteristic second derivative signal is observed but the quality of the trace is low and the signal-to-noise ratio rather poor. Many oscillations and hops are observed in this figure resulting from instabilities in the laser spectrum. This is confirmed by additional measurements of the laser spectrum made with the OSA. Figure 11b displays several measurements of the laser line successively acquired in a total timescale of a few tens of seconds (without any modulation on the laser). It is evident from this figure that the laser wavelength is not stable and moves by several gigahertz. This jitter is large compared to the typical width of 3 GHz (half width at half maximum) of the analyzed CO_2 line at atmospheric pressure and is responsible for the noise observed in the $2f$ spectrum (this spectrum was acquired in a timescale of ∼100 s, since the laser DC current is changed step-by-step in our driving electronics rather than ramped by a faster sawtooth waveform). Different factors may contribute to this spectral instability. Since the laser used in this experiment was packaged in an open TO can, i.e., not sealed with a protective window, it was first believed that mechanical noise on the membrane, due to vibrations, acoustic noise or air drafts, was the main origin of this problem. However, a simple model calculation of the "acoustic force" that would be required to cause the observed wavelength fluctuations shows that this assumption is not realistic: for a free spectral range of the cavity of $FSR \approx 5$ THz (corresponding to the effective cavity length $L_{\text{eff}} \approx 30$ μm), the membrane displacement needed to produce a typical frequency fluctuation $\Delta\nu = 10$ GHz (as observed in Fig. 11b) is $\Delta L = \Delta\nu \cdot \lambda/(2FSR) \cong 1.6$ nm. With a typical spring constant of the membrane of $k = 680$ N/m [23], the required force is $F = k\Delta L \approx 10^{-6}$ N. Using the area of the movable MEMS structure $A = 3.7 \times 10^{-8}$ m^2 (taking into account half of the beam length), a corresponding pressure $p = F/A = 28.7$ Pa is obtained. This value is by far too high to appear realistic so that acoustic noise cannot be the origin of the wavelength fluctuations observed in the laser spectrum.

Another possible reason for these instabilities is a fluctuation of the membrane bias current, since it was previously shown that the laser wavelength changes considerably with the membrane current (by many hundreds GHz/mA so that current noise of a few μA can induce frequency noise of >1 GHz). The use of a low-noise laser driver as a current source for the membrane bias current did not bring significant improvement on the laser wavelength stability. The noise spectral density of this current source, measured with

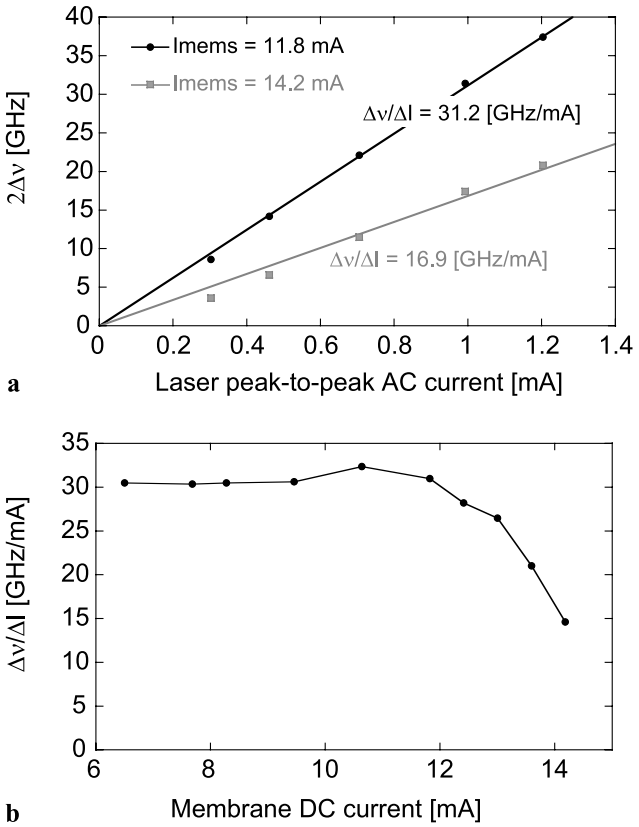

Fig. 9 (**a**) Amplitude of the laser FM as a function of the AC component of the injection current ($f = 25$ kHz) obtained for two different values of the MEMS bias current (at $I_{\text{laser}} = 21$ mA). (**b**) Influence of the membrane bias current on the laser FM response for a laser injection current modulation at $f = 25$ kHz ($I_{\text{laser}} = 21$ mA)

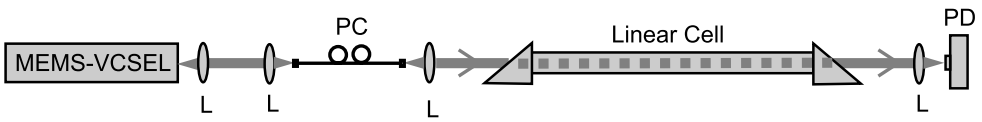

Fig. 10 Scheme of the optical setup used for preliminary gas sensing experiments. L: lens; PC: polarization controller; PD: photodiode. The polarization controller is used to have TM polarization on the Brewster-angled cell windows

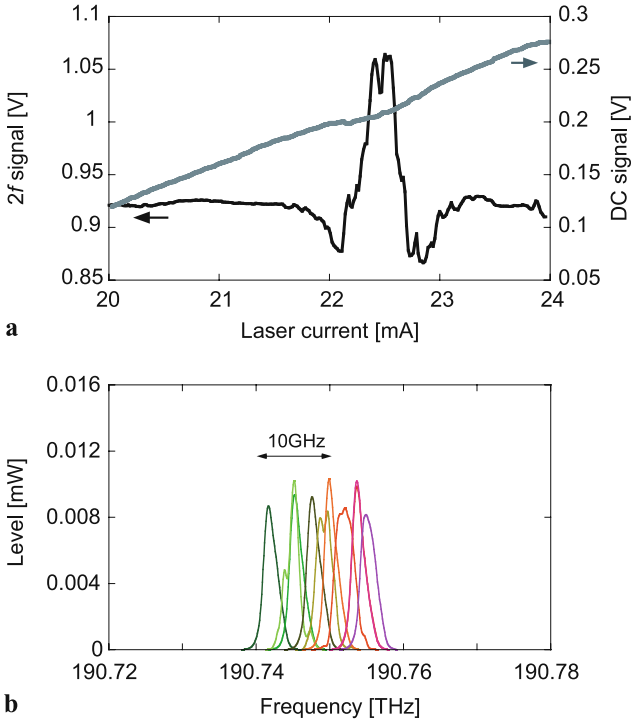

Fig. 11 (**a**) Direct absorption signal and $2f$ spectrum of a CO_2 line obtained when slowly scanning the laser via its injection current; $I_{\mathrm{MEMS}} = 14$ mA. (**b**) Successive measurements of the (unmodulated) laser spectrum obtained over a total timescale of a few tens of seconds showing large spectral instabilities of the laser; $I_{\mathrm{laser}} = 21$ mA; $I_{\mathrm{MEMS}} = 14$ mA

a FFT dynamic analyzer, has shown a dominant $1/f^{\alpha}$-type of noise at frequencies smaller than a couple of tens Hz. The power spectral density (PSD) of this low-frequency noise is described by $S_I(f) = K_I/f^{\alpha}$, where K is the current noise PSD at $f = 1$ Hz and α generally lies in the range $0 < \alpha < 2$ for $1/f$-type noise. A fit of the experimental current PSD in the range 0.1–30 Hz has shown a more pronounced frequency dependence with $\alpha \approx 2.6$ and $K_I \approx 1.5 \times 10^{-16}$ A^2/Hz at $I_{\mathrm{dc}} = 14$ mA. Accounting for a constant membrane tuning coefficient in this frequency range of approximately 750 GHz/mA as previously measured (see Fig. 8), these values translate into a frequency noise PSD $S_f(f) = K_f/f^{\alpha}$ with $K_f = 8.5 \times 10^{13}$ Hz^2/Hz. This low-frequency noise gives rise to a laser linewidth that depends on the observation time and which can be made arbitrarily large for long enough observation. This results from the divergence of the integral of the frequency noise PSD for $f \to 0$. A quantitative estimation of the influence of the observation time can be obtained by considering a finite low cut-off frequency $f_1 = 1/\tau$ in the integral, where τ is the observation time. By considering also $f_2 \to \infty$ for simplicity, the amplitude of the frequency fluctuations over an observation time τ is given by $\Delta f_{\mathrm{rms}} = \sqrt{K_f \tau^{\alpha-1}/(\alpha-1)}$. This leads to typical frequency fluctuations of 110 MHz over 10 s and 750 MHz over 100 s. This is clearly much smaller than the frequency fluctuations experimentally observed so that the current noise is not a significant contributor to the observed laser spectral instabilities.

Among the other possible sources of noise in our experiment, there are mechanical vibrations (transferred via the optical bench), which can have a severe effect on the membrane, as well as fluctuations of the membrane temperature due, for instance, to air drafts. A simple calculation has been performed to evaluate the membrane temperature fluctuation that is required to produce the 1.6-nm membrane displacement previously calculated. For this estimation, the geometry of the curved-mirror membrane with its supporting beams was approximated by a trapezoid (the mirror constitutes the short base of the trapezoid and the beams represent the legs). With a mean thermal expansion coefficient in the GaAs/AlGaAs DBR of $\alpha \approx 5.6 \times 10^{-6}$ K^{-1}, the expansion of one beam can be geometrically calculated in the right-angled triangle formed by the 6.1-μm air-gap altitude of the trapezoid and the $L_{\mathrm{beam}} = 89$ μm beam length (hypotenuse). If the air-gap increases by 1.6 nm, the hypotenuse needs to expand by $\Delta L_{\mathrm{beam}} = 110$ pm. This requires a temperature change $\Delta T = \Delta L_{\mathrm{beam}}/(\alpha L_{\mathrm{beam}}) \cong 0.2$°C. Such a temperature fluctuation of the membrane due to air drafts seems reasonably possible owing to the small thermal capacity of the membrane and to the fact that the laser package was open, i.e., not protected by a window. Therefore, we believe that this effect is the major contribution to the observed spectral instabilities of the laser and a better temperature stabilization of the membrane (e.g., by protecting it from air drafts using a package sealed with a protective window) should improve the laser stability.

5 Conclusion

A tunable MEMS-VCSEL made of a bottom InP-based semiconductor half-VCSEL and a top MEMS concave AlGaAs/GaAs mirror membrane has been extensively characterized with respect to its spectral, tuning, and modulation properties. A major objective of this work was to quantify important characteristics of this type of lasers for modulation-based spectroscopic detection techniques, such as WMS, in order to assess their suitability for gas sensing applications. The large tuning of MEMS-VCSELs offers new perspectives for compact and cost-effective multi-gas sensors and makes these lasers very attractive for such applications. The 20-nm continuous static tuning range obtained for the 1.56-μm MEMS-VCSEL used in this work is mainly limited by the absence of an AR coating on the top facet of the semiconductor half-VCSEL cavity, which makes the device operate in a semiconductor-coupled-cavity configuration, which is not favorable for large tunability. Tun-

ability enlarged by a factor of 3 has been previously obtained at the same wavelength with the use of an AR coating, so that significant improvement of our devices are expected in a near future in terms of tunability by using such an approach. Dynamic MEMS modulation showed a 3-dB bandwidth of 250 Hz, which is ∼40% higher than previous results obtained in anextended-cavity configuration. Finally, faster modulation capabilities have been shown when modulating the laser injection current. The corresponding injection-current-tuning coefficient was shown to be smaller compared to standard VCSELs and to be dependent on the membrane bias current, which is understandable by the fact that the injection current affects part of the laser cavity only, i.e., the semiconductor half-VCSEL. Anyway, the FM characteristics of the MEMS-VCSEL are fully suitable for WMS experiments both in atmospheric conditions and at reduced pressure.

Unfortunately, preliminary experiments of gas spectroscopy performed with this MEMS-VCSEL have been misleading due to insufficient spectral stability of the laser wavelength. Among the various possible sources of instability that have been evaluated either theoretically using simple model calculations (acoustic and thermal influence of air fluctuations) or experimentally (noise on the current source used to bias the membrane), thermal fluctuations of the membrane due to air drafts have been determined as a major contribution partly due to the open package used in this experiment. Mechanical vibrations transferred via the optical bench have also shown to produce instabilities in the membrane. The use of a laser mounted in a sealed packaged including a protective window and a better isolation of the experimental setup from mechanical vibrations constitute essential steps towards the achievement of quantitative spectroscopic results necessary to demonstrate the applicability of this MEMS-VCSEL in gas sensing.

Acknowledgement This work is supported by the European Commission via the EU project "Subtune" (FP7-ICT-224259) within the seventh Framework Programme.

References

1. M. Scotoni, A. Rossi, D. Bassi, R. Buffa, S. Iannotta, A. Boschetti, Appl. Phys. B **82**(3), 495 (2006)
2. M. Lackner, M. Schwarzott, F. Winter, B. Kögel, S. Jatta, H. Halbritter, P. Meissner, Opt. Lett. **31**(21), 3170 (2006)
3. B. Kögel, H. Halbritter, S. Jatta, M. Maute, G. Böhm, M.-C. Amann, M. Lackner, M. Schwarzott, F. Winter, P. Meissner, IEEE Sens. J. **7**(11), 1483 (2007)
4. M. Wippish, K.D. Dessau, Ind. Phys. **9**(3), 24 (2003)
5. Q.-V. Nguyen, R.W. Dibble, T. Day, Opt. Lett. **19**(24), 2134 (1994)
6. T. Day, in *Optical Fiber Communication Conference and Exhibit OFC 2001* (2001), pp. TuJ4-1–TuJ4-3
7. T. Sato, J. Lightwave Technol. **22**(7), 1782 (2004)
8. M. Pushkarsky, M. Weida, T. Day, in *Proc. of the Society of Photo-optical Instrumentation Engineers*, vol. 6871 (SPIE, Bellingham, 2008), pp. X8711–X8711
9. G. Wysocki, T. Tsai, S. So, Y. Wang, R. Lewicki, F.K. Tittel, D. Weidmann, Broadly tunable external cavity quantum cascade lasers and applications, in *Tunable Diode Laser Spectroscopy Conference*, July 13–17 2009, Zermatt, Switzerland, paper L2
10. C. Affolderbach, G. Mileti, Opt. Lasers Eng. **43**(3–5), 291 (2005)
11. B. Pezeshki, E. Vail, J. Kubicky, G. Yoffe, S. Zou, J. Heanue, P. Epp, S. Rishton, D. Ton, B. Faraji, M. Emanuel, X. Hong, M. Sherback, V. Agrawal, C. Chipman, T. Razazzan, IEEE Photonics Technol. Lett **14**(10), 1457 (2002)
12. C.-E. Zah, M.R. Amersfoort, B.N. Pathak, F.J. Favire, P.S.D. Lin, N.C. Andreadakis, A.W. Rajhel, R. Bhat, C. Caneau, M.A. Koza, J. Gamelin, IEEE J. Sel. Top. Quantum Electron. **3**(12), 584 (1997)
13. B. Kögel, M. Maute, H. Halbritter, F. Riemenschneider, G. Böhm, M.-C. Amann, P. Meissner, J. Opt. A: Pure Appl. Opt. **8**, S370 (2006)
14. F. Riemenschneider, M. Maute, H. Halbritter, G. Boem, M.C. Amann, P. Meissner, IEEE Photonics Technol. Lett. **16**(10), 2212 (2004)
15. R. Arndt, J. Appl. Phys. **36**(8), 2522 (1965)
16. J. Reid, D. Labrie, Appl. Phys. B **26**(3), 203 (1981)
17. G.C. Bjorklund, Opt. Lett. **5**(1), 15 (1980)
18. G.C. Bjorklund, M.D. Levenson, W. Lenth, C. Ortiz, IEEE J. Quantum Electron. **20**(9), 1045 (1984)
19. P. Debernardi, B. Kögel, K. Zogal, P. Meissner, M. Maute, M. Ortsiefer, G. Böhm, M.-C. Amann, IEEE J. Quantum Electron. **44**(4), 391 (2008)
20. M. Maute, B. Kögel, G. Böhm, P. Meissner, M.-C. Amann, IEEE Photonics Technol. Lett. **18**(5), 688 (2006)
21. A. Lytkine, W. Jäger, J. Tulip, Spectrochim. Acta A **63**(5), 940 (2006)
22. A. Lytkine, W. Jäger, J. Tulip, Proc. SPIE **5737**, 157 (2005)
23. B. Kögel, K. Zogal, S. Jatta, C. Grasse, M.-C. Amann, G. Cole, M. Lackner, M. Schwarzott, F. Winter, P. Meissner, Proc. SPIE **7266**, 72660O (2008). doi:10.1117/12.816272
24. H. Olesen, G. Jacobsen, IEEE J. Quantum Electron. **18**(12), 2069 (1982)